

Contents lists available at ScienceDirect

Journal of the Mechanical Behavior of Biomedical Materials

journal homepage: http://www.elsevier.com/locate/jmbbm





Rate-dependent adhesion of cartilage and its relation to relaxation mechanisms

Guebum Han^a, Melih Eriten^a, Corinne R. Henak^{a,b,c,*}

- ^a Department of Mechanical Engineering, University of Wisconsin-Madison, Madison, WI, USA
- ^b Department of Biomedical Engineering, University of Wisconsin-Madison, Madison, WI, USA
- ^c Department of Orthopedics and Rehabilitation, University of Wisconsin-Madison, Madison, WI, USA

ARTICLE INFO

Keywords: Cartilage Adhesion Fluid pressure Interfacial peeling Poroviscoelasticity

ABSTRACT

Cartilage adhesion has been found to play an important role in friction responses in the boundary lubrication regime, but its underlying mechanisms have only been partially understood. This study investigates the rate dependence of adhesion from pre-to post-relaxation timescales of cartilage and its possible relation to relaxation responses of the tissue. Adhesion tests on cartilage were performed to obtain rate-dependent cartilage adhesion from relaxed to unrelaxed states and corresponding relaxation responses. The rate dependence of cartilage adhesion was analyzed based on experimental relaxation responses. Cartilage adhesion increased about 20 times from relaxed to unrelaxed states. This rate-dependent enhancement correlated well with the load relaxation responses in a characteristic time domain. These experimental results indicated that the degree of recovery (or relaxation) in the vicinity of contact during unloading governed the rate dependence of cartilage adhesion. In addition, the experimentally measured enhancement of adhesion was interpreted with the aid of computationally and analytically predicted adhesion trends in viscoelastic, poroviscoelastic, and cohesive contact models. Agreement between the experimental and predicted trends implied that the enhancement of cartilage adhesion originated from complex combinations of interfacial peeling and negative fluid pressure generated within the contact area during unloading. These findings enhance the current understanding of rate-dependent adhesion mechanisms explored within short time scales and thus could provide new insight into friction responses and stick-induced damage in cartilage.

1. Introduction

Articular cartilage is a connective tissue composed of a fibrous solid matrix swollen by fluid. Collagen fibrils (around 15–22% of wet weight (Mow et al., 1992)) and proteoglycans (PGs) with glycosaminoglycan (GAG) side chains (around 4–7% of wet weight (Mow et al., 1992)) are the principal constituents of the solid matrix. Collagen fibrils mainly sustain tension (Andriotis et al., 2018; Kempson et al., 1968; Soulhat et al., 1999). Negatively charged GAGs produce intermolecular electrostatic repulsive forces and osmotic swelling pressure, contributing to compressive resistance of cartilage (Han et al., 2011; Mow et al., 1992). Osmotic swelling pressure is counterbalanced by tensile resistance of collagen fibrils (Han et al., 2011). Fluid accounts for around 60–85% of wet weight of cartilage and swells collagen fibrils and pore space in the solid matrix (Maroudas et al., 1991; Mow et al., 1992; Torzilli, 1985). Interplays of these constituents provide rate-dependent mechanical,

dissipative, and tribological responses of articular cartilage (Han et al., 2018; Nia et al., 2015, 2011), ultimately protecting diarthrodial joints under various loading conditions.

Cartilage adhesion has a pronounced effect on friction responses of cartilage in the boundary lubrication regime. Kinetic (sliding) friction forces measured on cartilage increased with increasing adhesion energy (Coles et al., 2008). Cartilage adhesion and friction were region-dependent and interdependent; cartilage from high-load-bearing locations exhibited higher adhesion and kinetic (sliding) friction forces than that from low-load-bearing locations (Chan et al., 2011). Cartilage adhesion increased with progressive relaxation, and static (stick) friction of cartilage linearly correlated with the magnitude of adhesion (Han and Eriten, 2018). The relation between cartilage adhesion and friction in the boundary lubrication regime indicated that understanding of cartilage adhesion can provide new insight into potential causes of severe surface damage in stick-slip sliding regimes, accompanying high

^{*} Corresponding author. Department of Mechanical Engineering, University of Wisconsin-Madison, Madison, WI, USA. *E-mail addresses*: ghan28@wisc.edu (G. Han), eriten@wisc.edu (M. Eriten), chenak@wisc.edu (C.R. Henak).

friction peaks, compared to smooth sliding regimes (Lee et al., 2013). An investigation into cartilage adhesion can also provide possible origins of friction-induced high shear strains near the articular surfaces (Wong et al., 2008), which could lead to cell death (Bonnevie et al., 2018). In addition, considering cartilage and hydrogels have ultrastructural similarities in the context of the solid matrixes swollen by fluid, a previous study on hydrogel interfaces showed that relaxation-dependent adhesion governed friction responses (Reale and Dunn, 2017).

The origins of cartilage adhesion are not fully understood. Cartilage adhesion is highly dependent on the degree of relaxation in the tissue (Han and Eriten, 2018) which is described with poroelastic (PE) and viscoelastic (VE) responses (Han et al., 2018; Lai and Hu, 2017; Mak, 1986; Nia et al., 2011). These observations, combined with previous studies on cartilage-like materials, hinted that cartilage adhesion could be directly linked to relaxation processes. A recent study showed that adhesion of hydrogels was relaxation-dependent and originated from PE relaxation-driven fluid pressure within the contact area (Reale and Dunn, 2017). This is referred to as suction effect (Reale and Dunn, 2017). Relaxation-driven fluid pressure is expected to contribute to cartilage adhesion as well. Indeed, fluid pressure in cartilage was predicted to fluctuate from negative to positive values under cyclic unconfined compression at relatively low loading rates (0.001-0.01 Hz for cartilage with a radius of 1.5 mm) (Suh, 1996). In addition, previous studies on soft elastomers, exhibiting VE relaxation responses similar to cartilage, revealed that adhesion of elastomers exhibited strong dependence on unloading rates (Ahn and Shull, 1996; Barthel and Frétigny, 2009; Cai et al., 2015; Deruelle et al., 1995; Yamaguchi et al., 2018). The rate dependence of adhesion was explained by introducing rate-dependent interfacial phenomena through a cohesive zone at the edge of the contact area (Barthel and Frétigny, 2009), treating the elastomeric adhesive contact problem as crack propagation across a VE interface. These previous studies on adhesion of soft materials with relaxation responses similar to cartilage suggested that underlying mechanisms of rate-dependent cartilage adhesion can be understood in the context of the PE relaxation-driven fluid pressure, VE relaxation, and rate-dependent interfacial peeling.

Rate-dependent mechanical responses of cartilage are well known to stem from combined effects of poroviscoelastic (PVE) relaxation responses (Han et al., 2018; Lai and Hu, 2017; Mak, 1986; Nia et al., 2011). These relaxations are observed experimentally (Chiravarambath et al., 2008; Han et al., 2018; Huang et al., 2003, 2001), and thus are commonly employed in finite element (FE) modeling of cartilage (Chiravarambath et al., 2008; DiSilvestro et al., 2000; Han et al., 2019; Huang et al., 2003; Wilson et al., 2005). However, the link between rate-dependent adhesion and PVE relaxation responses in the tissue is not established. The absence of experimental observation of rate-dependent cartilage adhesion over a broad range of unloading rates is a major factor that limits the current understanding of this link.

The objective of this study is to investigate rate-dependent adhesion and mechanics of cartilage over a broad range of loading/unloading rates and relate the tissue relaxation responses to the enhancement of adhesion. In particular, the adhesive strength in cartilage is measured by probe tack tests at unloading rates ranging from fully relaxed to fully unrelaxed tissue states. Relaxation responses of cartilage are also monitored from the holding periods of the corresponding adhesion tests. Possible correlations between the rate dependence of adhesion and the mechanical responses of the tissue are examined in a normalized characteristic time domain. Underlying mechanisms responsible for the rate-dependent enhancement of cartilage adhesion are further investigated by comparing the experimental observations with the predictions of FE and cohesive zone models.

2. Methods

2.1. Sample preparation

Four full-thickness cartilage samples were obtained from four patellae of porcine joints acquired from a local abattoir (4 animals, 5–6 months old, sex unknown and assumed random). Cylindrical cores with a diameter of 6 mm were obtained by a biopsy punch and a scalpel. A microtome was used to remove subchondral bone and generate a deep surface parallel to articular surface, which allowed indentations to be perpendicular to the articular surface. The deep zone of each sample was fixed to a Petri dish via cyanoacrylate (Loctite 495, Henkel, Germany). Samples were kept hydrated during preparation and testing in Dulbecco's phosphate-buffered saline (DPBS) with a protease inhibitor (PI).

2.2. Measurement of adhesion and load relaxation response

Pull-off forces, $F_{\text{pull-off}}$, apparent work of adhesion, γ_{Exp} , and load relaxation responses were acquired by performing adhesion tests on articular surface. Tests were conducted on a Bruker TI 950 TriboIndenter (Bruker, Eden Prairie, MN) with a sapphire spherical indenter (tip radius, R = 1 mm). A displacement of 60 μ m was applied at a loading rate of $100 \,\mu\text{m/s}$, held for $100 \,\text{s}$, and then removed at unloading rates of 3^0 , 3^1 , 3^2 , 3^3 , 3^4 , 3^5 , and $3^6 \,\mu\text{m/s}$ (Fig. 1a). This wide range of unloading rates was employed to measure $F_{\text{pull-off}}$ and γ_{Exp} at time scales faster (e.g., $3^6 \mu m/s$) and slower (e.g., $3^0 \mu m/s$) than the apparent relaxation time of cartilage at the experimental contact length scale; this selection of unloading rates is revisited in the discussion section. There were 12 total measurements at each unloading rate and the averages and standard deviations were reported; three different locations per sample were tested at each rate and four samples were prepared from four different animals (Section 2.1). F_{pull-off} was defined as the maximum negative force of a load-displacement curve (Fig. 1b and c). $F_{\text{pull-off}}$ was converted to γ_{Exp} using the Johnson-Kendall-Roberts (JKR) contact model (Johnson et al., 1971):

$$\gamma_{\rm Exp} = -\frac{F_{\rm pull-off}}{1.5\pi R}.\tag{1}$$

The average load relaxation response, $F_{\rm relax}(t)$, was defined as the average load-time curve (84 curves) during the holding period of the adhesion testing (Fig. 2a). For example, $F_{\rm relax}(0)$ corresponds to the peak value of the average experimental load-time curve (Fig. 2a).

2.3. Possible link between rate dependence of cartilage adhesion and relaxation response

The rate dependence of cartilage adhesion was examined through the correlation between $\gamma_{\rm Exp}$ and $F_{\rm relax}(t)$ in a normalized characteristic time domain by an apparent relaxation time constant, $\tau_{\rm relax}$. $\gamma_{\rm Exp}$ at different unloading rates were normalized using the time to achieve $F_{\rm pull-off}$ from the initiation of unloading, $t_{\rm pull-off}$, and $\tau_{\rm relax}$ as follows:

$$\frac{\gamma_{\rm Exp}}{\left({\rm Avg.} \quad \gamma_{\rm Exp}\right)_{min}} = \Delta \gamma_{\rm Exp}(\bar{t}_{\rm R}) = \Delta \gamma_{\rm Exp}\left(\frac{t_{\rm pull-off}}{\tau_{\rm relax}}\right) \tag{2}$$

where (Avg. $\gamma_{\rm Exp}$)_{min} is the minimum value of average $\gamma_{\rm Exp}$ at different loading rates and $t_{\rm pull\text{-}off}$ was calculated by dividing critical displacements, $D_{\rm pull\text{-}off}$, with corresponding unloading rates. $D_{\rm pull\text{-}off}$ was defined as the displacement required to reach $F_{\rm pull\text{-}off}$ from the initiation of unloading. The normalized form of $\Delta\gamma_{\rm Exp}$ in Eq. (2) represents the experimentally measured enhancement of cartilage adhesion. Then, $F_{\rm relax}(t)$ was normalized using $\tau_{\rm relax}$ as follows:

$$\frac{F_{\text{relax}}(t) - F_{\text{relax}}(\infty)}{F_{\text{relax}}(0) - F_{\text{relax}}(\infty)} = \overline{F}_{\text{relax}}(\overline{t}_{R}) = \overline{F}_{\text{relax}}\left(\frac{t}{\tau_{\text{relax}}}\right)$$
(3)

where $F_{\rm relax}$ (0) and $F_{\rm relax}$ (∞) are the loads at the unrelaxed and relaxed

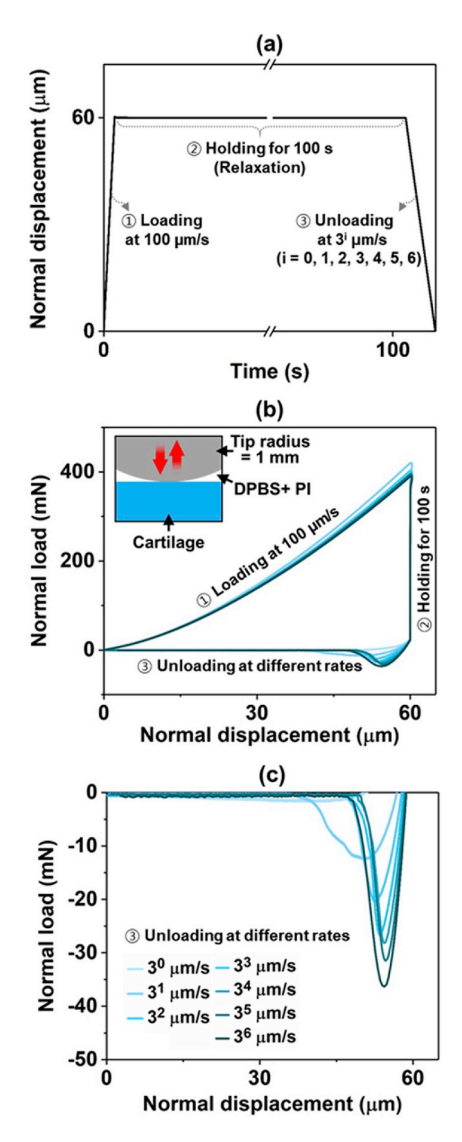


Fig. 1. Representative (a) loading-holding-unloading profiles used to measure adhesion and relaxation responses and (b and c) load-displacement curves from corresponding profiles ((b): loading, holding, and unloading portions and (c): unloading portions). In (c), the maximum absolute values of forces are defined as $F_{\text{pull-off}}$. The average relaxation response measured from the holding portion, $F_{\text{relax}}(t)$, is presented in Fig. 2a.

states, respectively. $F_{\rm relax}$ (0) was a peak value of $F_{\rm relax}$ (t) (Fig. 2a). $F_{\rm relax}$ (~25 s) was considered as the sufficiently-relaxed state as the load relaxation after t=~25 s was negligible compared to the major relaxation in the beginning; i.e., load relaxation rate at t=25 s was 0.1 mN/s «35 mN/s at t=10 s (Fig. 2a). $\tau_{\rm relax}$ was estimated to be 1.81s by fitting a single exponential decay function, $F_{\rm relax}^*(t)$, to $F_{\rm relax}(t)$ (0 \leq t \leq ~25 s, Fig. 2a). The detailed process of determining $\tau_{\rm relax}$ is provided in the supplementary material. The purpose of the comparison between $\Delta \gamma_{\rm Exp}$ ($t_{\rm R}$) and $t_{\rm relax}$ ($t_{\rm R}$) was to correlate cartilage adhesion ($t_{\rm relax}$) and the apparent relaxation response ($t_{\rm relax}$) across the same time scales relevant to mechanical loading/unloading.

2.4. Interpretation of enhancement of cartilage adhesion via various contact models

Mechanisms underlying cartilage adhesion were investigated by comparing the experimentally observed enhancement of adhesion to the enhancements predicted by three contact models employing different rate-dependent mechanisms in the bulk material and at the interface.

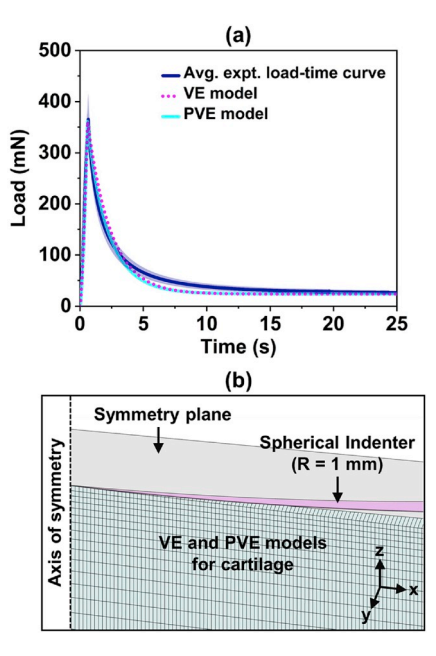


Fig. 2. (a) Comparison between average experimental and FE-predicted load-time curves and (b) spherical indenter (rigid body) and cartilage (VE and PVE models) for FE modeling. The relaxation response of the average experimental load-time curve was defined as $F_{\rm relax}(t)$. The shaded area shows the standard deviation. The VE and PVE models were tuned based on the average experimental load-time curve. The detailed description of the boundary and contact conditions for the FE models is provided in the supplementary material.

The enhancements of adhesion by the relaxation responses of the bulk material were predicted through FE models with VE and PVE relaxation (Section 2.4.1). The enhancement of adhesion by rate-dependent interfacial phenomena was predicted through a rate-dependent cohesive zone model proposed by Barthel and Fre tigny (Barthel and Frétigny, 2009) (Section 2.4.2).

2.4.1. FE modeling to predict enhancements of adhesion by bulk material responses

An axisymmetric FE model of the indenter-sample system (wedge angle of $3^\circ,$ Fig. 2b) was developed to further understand the experimentally measured adhesive responses of cartilage at different loading rates. Geometry and loading matched the experimental setup, with the average thickness of tested cartilage samples $(1.52\pm0.09\,\mathrm{mm})$ and a relativley large $1.5\,\mathrm{mm}$ radius to eliminate possible boundary effects. Cartilage was discretized with a combination of 8-node linear hexahedral (14450 elements) and 6-node linear pentahedral (50 elements) elements. The number of elements required was determined by mesh convergence analysis. Meshing was biased towards to contact area resulting in the smallest elements within a radius of $0.3\,\mathrm{mm}$ from the symmetry axis.

Sticky (tied) contact was used between the indenter and cartilage. This contact condition ensured decoupling of interfacial effects (i.e., contact peeling) from the relaxation responses of a material during unloading. As a result, this assumed that adhesion up to $D_{\rm pull-off}$ and $F_{\rm pull-off}$ dominantly originated from the relaxation responses of a material rather than the interfacial responses. The loading-holding-unloading profiles used for the transient FE analyses corresponded to the experimental adhesion tests (Fig. 1a). The indenter and cartilage were modeled in SolidWorks (2017), Gmesh (Geuzaine and Remacle, 2009), and PreView version 1.20.2, respectively.

Cartilage was modeled with VE and PVE models, and an indenter was modeled as a rigid body (Fig. 2b). The VE model was generated by combining a neo-Hookean material (elastic modulus, $E_{\rm VE}=$ fitting parameter, and Poisson's ratio, $\nu=0.3$ (Li et al., 2008)) and a VE

relaxation with an exponential decay function (single relaxation time constant, $\tau = 1.8$ s (Yang et al., 2012), and VE coefficient, $\rho_{\rm VE} =$ fitting parameter). The PVE solid was generated by adding PE relaxation to the VE solid composed of a neo-Hookean material (elastic modulus, E_{PVE} = fitting parameter, and Poisson's ratio, v = 0.3 (Li et al., 2008)) and a VE response with an exponential decay function (relaxation time constant, $\tau = 1.8$ s (Yang et al., 2012), and VE coefficient, $\rho_{PVE} = \text{fitting}$ parameter). PE relaxation was modeled via Holmes-Mow strain-dependent permeability ($k_0 = 0.0027 \text{ mm}^4/\text{N}$ (Ateshian et al., 1997), power-law exponent, M = 2.2 (Ateshian et al., 1997), and power-law exponent, $\alpha_{perm} = 2$ (Ateshian et al., 1997)). All constitutive models were used as implemented in FEBio version 2.5.2. The definitions of the material parameters in the models are presented in the supplementary material. The fitting parameters of the VE (E_{VE} and ρ_{VE}) and PVE (E_{PVE} and ρ_{PVE}) models were determined by fitting the FE-predicted load-time curves to the average experimental load-time curve (Fig. 2a, $R^2 = 0.95 - 0.97$ based on average load relaxation curve, $F_{\text{relax}}(t)$ ($0 \le t \le$ \sim 25 s)); the relaxation behavior of cartilage was attributed to an apparent VE relaxation for the VE model and PVE relaxations for the PVE model. The average curve was obtained as the mean of 84 load relaxation curves from adhesion tests, paired with the measurement results of adhesion. The determined fitting parameters were $E_{
m VE} = 0.93\,{
m MPa}$ and $ho_{
m VE}~=16.3$ for the VE model and $E_{
m PVE}~=0.87\,{
m MPa}$ and $ho_{\mathrm{PVE}} = 13.6$ for the PVE model. The spherical indenter tip was made of sapphire, and thus was modeled as a rigid and impermeable body. The FE simulations were conducted in FEBio version 2.5.2 (Maas et al.,

FE-predicted adhesion was obtained by applying the loading-holding-unloading profile of adhesion tests to FE models and predicting pull-off forces ($F_{\rm Matl-VE-pull-off}$ for the VE model and $F_{\rm Matl-VE-pull-off}$ for the PVE model) at the experimentally determined $D_{\rm pull-off}$. $F_{\rm Matl-VE-pull-off}$ was obtained by integrating the stress in the z direction within the fully-adhered contact area at $D_{\rm pull-off}$ and was converted to work of adhesion, $\gamma_{\rm Matl-VE}$, via Eq. (1). Therefore, $\gamma_{\rm Matl-VE}$ represents work of adhesion due to the apparent VE response of the material with no contributions from interfacial peeling. $F_{\rm Matl-PVE-pull-off}$ was calculated by integrating the fluid pressure built-up within the fully-adhered contact area at $D_{\rm pull-off}$ and was converted to work of adhesion, $\gamma_{\rm Matl-FP-PVE}$, through Eq. (1). Thus, $\gamma_{\rm Matl-FP-PVE}$ accounts for adhesion stemming from relaxation-driven fluid pressure (i.e., suction effect) within the contact area, again with no contributions from interfacial phenomena.

2.4.2. Cohesive zone model to predict enhancement of adhesion by interfacial response

The effect of interfacial peeling on rate-dependent cartilage adhesion was investigated by a cohesive zone model proposed by Barthel and Fre tigny (Barthel and Frétigny, 2009). In this model, a rate-dependent adhesive contact problem between a sphere and a flat surface was considered to be a crack growth problem across a cohesive zone at the contact edge. In particular, fast peeling at contact allows for very little normal separation at the contact edge (i.e., crack tip) when compared to slower peeling cases. Therefore, the crack tip area experiencing stresses close to cohesive strength is smaller for slower peeling rates, and increases with peeling rates. In the physical extreme of peeling at a fully relaxed state (i.e., quasi-static crack growth), the critical cohesive stresses lead to very large crack tip opening displacements because of a reduced modulus, and thus the cohesive zone size is minimized. One of the major assumptions of this model is that rate effects in the bulk deformation are negligible compared to the rate dependence of the crack tip deformation. This assumption enabled Barthel and Fre tigny to obtain a simple analytical expression for the rate-dependent enhancement of adhesion by interfacial peeling, $\Delta \gamma_{\text{Intf-CZ}}$ (Barthel and Frétigny, 2009). $\Delta \gamma_{\text{Intf-CZ}}$ was calculated using the experimental relaxation response $(F_{\text{relax}}(t))$ as explained in the remainder of this section and is defined as follows:

$$\Delta \gamma_{\text{Intf-CZ}}(t_r) = \frac{\varepsilon(t_r)}{\varepsilon_{\infty}} = \frac{J_{\text{eff}}(\infty)}{J_{\text{eff}}(t_r)}$$
(4)

where t_r is the time required for the moving crack to cross the cohesive zone, $\varepsilon(t_r)$ is the size of the cohesive zone at t_r , ε_∞ is the minimum size of the cohesive zone at a low crack velocity (i.e., relaxed state), and $J_{eff}(\infty)$ and $J_{eff}(t_r)$ were the effective compliance functions at infinite and arbitrary times, respectively. $J_{eff}(t)$ is defined as follows (Barthel and Frétigny, 2009):

$$J_{eff}(t) = \frac{2}{t^2} \int_0^t (t - \tau) J(\tau) d\tau$$
 (5)

where $J(\tau)$ is the creep function. J(t) can be obtained from the reduced relaxation modulus, $E^*(t)$, and $E^*(t)$ can be expressed as follows:

$$E^{*}(t) = E_{ea} + E_{in}e^{\frac{-t}{\tau_{\text{relax}}}} \tag{6}$$

where E_{in} is the instantaneous modulus, E_{eq} is the equilibrium modulus, and $\tau_{\rm relax}$ is the apparent relaxation time. E_{in} , E_{eq} , and $\tau_{\rm relax}$ were determined to be 17.35 MPa, 1.3 MPa, and 1.81 s, respectively. $E^*(t)$ was determined based on the average load relaxation response ($F_{\rm relax}(t)$) and the detailed process of determining $E^*(t)$ is provided in the supplementary material. Then, $J(\tau)$ can be expressed with E_{in} , E_{eq} , and $\tau_{\rm relax}$ as follows (Lakes, 2009):

$$J(t) = \frac{1}{E_{eq}} - \frac{E_{in}}{E_{eq}(E_{in} + E_{eq})} e^{\frac{-t}{r_{\text{recep}}}}$$
(7)

with

$$\tau_{\text{creep}} = \tau_{relax} \frac{\left(E_{in} + E_{eq}\right)}{E_{ra}} \tag{8}$$

where τ_{creep} is the creep time. $J(\tau)$ is calculated to be 0.77 - 0.72 $e^{\frac{-t}{22.597}}$. Finally, $\Delta\gamma_{\text{Intf-CZ}}$ (Eq. (4)) can be obtained by using $J_{eff}(t)$ (Eq. (5)) and J(t) (Eq. (7)). In summary, $\Delta\gamma_{\text{Intf-CZ}}$ represents the enhancement of adhesion originating from rate-dependent interfacial peeling, and the rate dependence of interfacial peeling was obtained based on the apparent relaxation behavior of cartilage.

2.4.3. Comparison between experimental and predicted enhancements of adhesion

The experimental adhesion was compared to the adhesion predicted by the FE and analytical models. The comparison was conducted in a normalized adhesion-time domain, representing the enhancement of adhesion in a normalized characteristic time domain. The experimental enhancement of adhesion was expressed as $\Delta\gamma_{\rm Exp}\left(f_{\rm R}\right)$ as presented in Eq. (2). Similarly, the adhesion values predicted by the FE simulations ($\gamma_{\rm Matl-FP-PVE}$) were normalized with their minimum values and $\tau_{\rm relax}$ as follows:

$$\frac{\gamma_{i}}{(\gamma_{i})_{min}} = \Delta \gamma_{i}(\bar{t}_{R}) = \Delta \gamma_{i}\left(\frac{t_{pull-off}}{\tau_{relax}}\right)$$
(9)

where i corresponds to Matl-VE for $\gamma_{Matl-VE}$ and Matl-FP-PVE for $\gamma_{Matl-FP-PVE}$, respectively. Since the adhesion predicted by the analytical cohesive zone model (Barthel and Frétigny, 2009) was already calculated as normalized adhesion (Eq. (4)), its time scale, t_r , was only additionally normalized by τ_{relax} into a normalized time domain, \bar{t}_R , as follows:

$$\Delta \gamma_{\text{Intf-CZ}}(\bar{t}_{R}) = \Delta \gamma_{\text{Intf-CZ}}\left(\frac{t_{r}}{\tau_{\text{relax}}}\right). \tag{10}$$

The normalized time domain used in Eqs. (2), (9) and (10) compared $t_{\text{pull-off}}$ with t_{r} ; the validation of this comparison will be revisited in the discussion section. These enhancements of adhesion predicted by the rate-dependent mechanisms ($\Delta \gamma_{\text{Matl-VE}}$, $\Delta \gamma_{\text{Matl-FP-PVE}}$, and $\Delta \gamma_{\text{Intf-CZ}}$) aided

in interpreting the relative importance of bulk and interface mechanics on the enhancement of cartilage adhesion ($\Delta\gamma_{Exp}$) from relaxed to unrelaxed states. Specifically, $\Delta\gamma_{Matl\cdot VE}$ and $\Delta\gamma_{Matl\cdot FP\cdot PVE}$ gauged the effect of the relaxation responses of the bulk material on $\Delta\gamma_{Exp}$ while $\Delta\gamma_{Intf\cdot CZ}$ evaluated the influence of the interfacial responses (i.e., contact peeling) on $\Delta\gamma_{Exp}$.

2.5. Statistical analysis

The Kruskal-Wallis test (nonparametric test) was used to statistically examine the rate dependence of $F_{\rm pull-off}$, $t_{\rm pull-off}$, and $D_{\rm pull-off}$. All statistical analysis was performed using MATLAB (The MathWorks, Inc., Natick, MA). A significance level of 5% was used for all tests.

3. Results

Cartilage adhesion exhibited strong dependence on unloading rates ($F_{\rm pull-off}$ and $\gamma_{\rm Exp}$, $p=1.1\times 10^{-14}$) (Fig. 3a). $F_{\rm pull-off}$ showed a rapid increase at relatively slow unloading rates (3^0-3^4 µm/s) and gradually settled at a peak value at the fastest unloading rate (3^6 µm/s). $F_{\rm pull-off}$ at 3^4 µm/s was about 15.21 times $F_{\rm pull-off}$ at 3^0 µm/s, and $F_{\rm pull-off}$ at 3^6 µm/s was about 1.31 times $F_{\rm pull-off}$ at 3^4 µm/s. As $\gamma_{\rm Exp}$ is proportional to $F_{\rm pull-off}$ (Ep. 1), the rate dependence of $\gamma_{\rm Exp}$ is identical to $F_{\rm pull-off}$. $\gamma_{\rm Exp}$ at unloading rates of 3^0 , 3^4 , and 3^6 µm/s were 0.36 ± 0.15 , 5.49 ± 0.43 , and 7.16 ± 0.54 J/m², respectively.

The time ($t_{\rm pull-off}$) and distance ($D_{\rm pull-off}$) required for $F_{\rm pull-off}$ were also rate-dependent ($p=1.91\times10^{-15}$ for $t_{\rm pull-off}$ and $p=3.97\times10^{-11}$ for $D_{\rm pull-off}$) (Fig. 3b and c). $t_{\rm pull-off}$ abruptly decreased at relatively slow

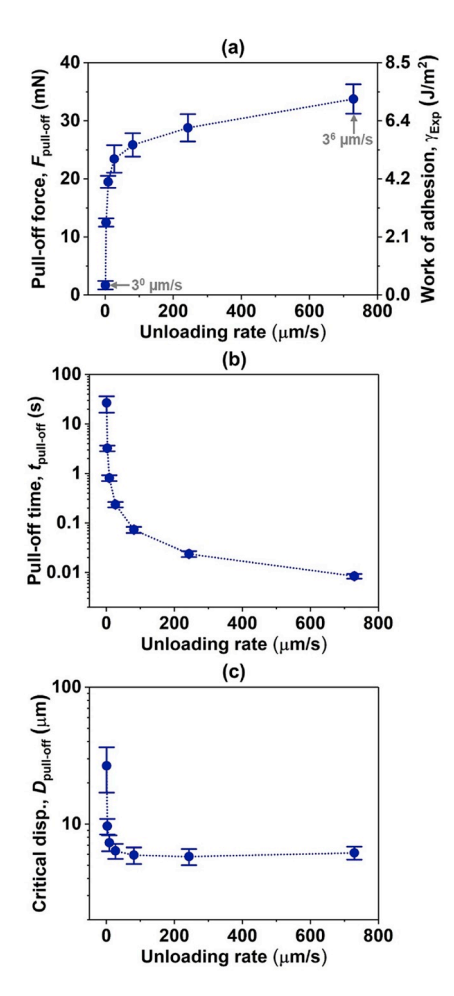


Fig. 3. Results of adhesion tests at different unloading rates: (a) $F_{\rm pull-off}$ and $\gamma_{\rm Exp}$, (b) $t_{\rm pull-off}$, and (c) $D_{\rm pull-off}$. The error bars show the standard deviations.

unloading rates (i.e., 3^0 – 3^4 µm/s), and gradually decreased at relatively fast unloading rates (i.e., 3^4 – 3^6 µm/s) (Fig. 3b). $t_{\rm pull\text{-}off}$ at 3^4 µm/s was about 0.27% of $t_{\rm pull\text{-}off}$ at 3^0 µm/s, and $t_{\rm pull\text{-}off}$ at 3^6 µm/s was about 11.56% of $t_{\rm pull\text{-}off}$ at 3^4 µm/s. Similarly, $D_{\rm pull\text{-}off}$ suddenly dropped in the relatively slow unloading regimes and became stable in the relatively fast unloading regimes (Fig. 3c). $D_{\rm pull\text{-}off}$ at 3^4 µm/s was about 22.23% of $D_{\rm pull\text{-}off}$ at 3^0 µm/s, and $D_{\rm pull\text{-}off}$ at 3^6 µm/s was about 104.01% of $D_{\rm pull\text{-}off}$ at 3^4 µm/s.

The rate dependence of $\gamma_{\rm Exp}$ correlated closely with $F_{\rm relax}(t)$ (Fig. 4). The comparison between $\gamma_{\rm Exp}$ and $F_{\rm relax}(t)$ was conducted in the normalized domain (Eq. (2) and (3)). In particular, the normalized time ($\bar{t}_{\rm R}$) allowed the comparison between $\Delta\gamma_{\rm Exp}$ and $\bar{F}_{\rm relax}$ as a function of the characteristic times ($t_{\rm pull-off}$ for $\Delta\gamma_{\rm Exp}$ and relaxation time for $\bar{F}_{\rm relax}$) relative to $\tau_{\rm relax}$ (=1.81s). The transition period of $\Delta\gamma_{\rm Exp}(\bar{t}_{\rm R})$ was consistent with that of $\bar{F}_{\rm relax}(\bar{t}_{\rm R})$, and $\Delta\gamma_{\rm Exp}$ at 30 µm/s and 36 µm/s corresponded to the relaxed and unrelaxed states of $\bar{F}_{\rm relax}(\bar{t}_{\rm R})$, respectively (Fig. 4a and b). Consequently, $\Delta\gamma_{\rm Exp}$ strongly correlated with $\bar{F}_{\rm relax}$ at corresponding $\bar{t}_{\rm R}$ (${\rm R}^2=0.94$) (Fig. 4c).

The experimentally measured enhancement of adhesion ($\Delta \gamma_{Exp}$) was

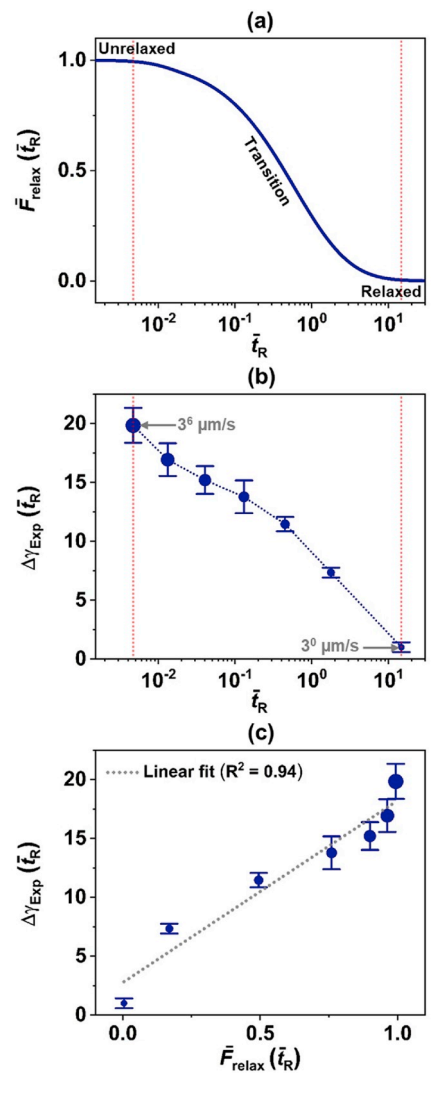


Fig 4. (a) $\overline{F}_{\rm relax}$ ($\overline{t}_{\rm R}$) and (b) $\Delta\gamma_{\rm Exp}(\overline{t}_{\rm R})$ and (c) correlation between $\overline{F}_{\rm relax}$ ($\overline{t}_{\rm R}$) and $\Delta\gamma_{\rm Exp}$ ($\overline{t}_{\rm R}$) at corresponding $\overline{t}_{\rm R}$. The characteristic times ($t_{\rm pull-off}$ for $\Delta\gamma_{\rm Exp}$ and relaxation time for $\overline{F}_{\rm relax}$) were normalized with $\tau_{\rm relax}$ (=1.81 s) (Eq. (2) and (3)). In (b) and (c), the size of a symbol reflects the magnitude of loading rate (e.g., the smallest size: 3^0 μm/s and the largest size: 3^6 μm/s). The error bars show the standard deviations.

not completely consistent with the enhancements of adhesion predicted by the various rate-dependent mechanisms ($\Delta \gamma_{Matl-VE}$, $\Delta \gamma_{Matl-FP-PVE}$, and $\Delta \gamma_{\text{Intf-CZ}}$) (Fig. 5). In order to interpret possible mechanisms governing cartilage adhesion, $\Delta \gamma_{Exp}$ was compared in the normalized time domain with the enhancements predicted by $\Delta \gamma_{\text{Matl-VE}}$, $\Delta \gamma_{\text{Matl-FP-PVE}}$, and $\Delta \gamma_{\text{Intf-}}$ cz. The maximum enhancement measured by the adhesion tests, $(\Delta \gamma_{\rm Exp})_{\rm max}$, was about 20 times, and $\Delta \gamma_{\rm Exp}$ increased in a linear fashion on a logarithmic time scale (Fig. 5). The maximum enhancement predicted by the apparent VE relaxation of a material, $(\Delta \gamma_{Matl-VE})_{max}$, was about 4 times, which was much lower than $(\Delta \gamma_{Exp})_{max}$. $\Delta \gamma_{Matl-VE}$ showed an increasing trend in the relatively slow loading rates (i.e., $3^0 \, \mu m/s$ - $3^2 \mu m/s$) and a stable trend in the relatively fast loading rate (i.e., $3^2 \mu m/s$) s – $3^6 \mu m/s$) (Fig. 5). This trend of $\Delta \gamma_{Matl-VE}$ was not consistent with that of $\Delta \gamma_{Exp}$. The maximum enhancement predicted by PVE relaxationdriven fluid pressure within the contact area, (Δγ_{Matl-FP-PVE})_{max}, was about 14 times, and hence, $(\Delta \gamma_{\text{Matl-FP-PVE}})_{\text{max}}$ was closer to $(\Delta \gamma_{\text{Exp}})_{\text{max}}$ in comparison with $(\Delta \gamma_{\text{Matl-VE}})_{\text{max}}$. $\Delta \gamma_{\text{Matl-FP-PVE}}$ linearly increased on a logarithmic time scale (Fig. 5), and this trend was consistent with $\Delta \gamma_{\rm Exp}$ over a wide range of unloading rates. The maximum enhancement of about 15 times is predicted by the interfacial peeling, $(\Delta \gamma_{Intf-CZ})_{max}$. A rapid increase of $\Delta \gamma_{Intf-CZ}$ was consistent with that of $\Delta \gamma_{Exp}$ in the relatively slow loading rates (i.e., $3^0 \, \mu \text{m/s} - 3^4 \, \mu \text{m/s}$), but $\Delta \gamma_{\text{Intf-CZ}}$ reached a steady value after around 3⁴ µm/s and deviated from an increasing trend of $\Delta \gamma_{\rm Exp}$ in the relatively fast loading rate (i.e., $3^5 \, \mu \rm m/s - 3^6 \, \mu \rm m/s$); this overall trend of $\Delta \gamma_{\text{Intf-CZ}}$, reaching a plateau, was similar to that of $\Delta \gamma_{\text{Matl-}}$ VE. In summary, none of the bulk-only or interface-only mechanisms could explain the adhesion enhancement trends we observed experimentally. Nevertheless, agreement between experimental and predicted results observed in Fig. 5 suggested that a model coupling the PE relaxation-driven suction effect in the bulk and the VE effects at the interface could explain the measured rate-dependence of cartilage adhesion.

4. Discussion

Recovery degree of cartilage in the vicinity of the indenter was the driving factor behind the rate dependence of adhesion ($F_{\rm pull-off}$ and $\gamma_{\rm Exp}$). The load relaxation curve (Fig. 2a) showed that about 63% of the total relaxation (about 340 mN) was completed after $\tau_{\rm relax}=1.81$ s. Cartilage relaxation was likely to proceed with progressive dehydration within the contact region (i.e., fluid diffusion) (PE relaxation) (Han et al., 2018; Nia et al., 2015, 2011) and rearrangement of macromolecules (intrinsic VE relaxation) (Han et al., 2019, 2018; Nia et al., 2015). Since the unloading was applied after a relaxation period of 100 s, which is much larger than $\tau_{\rm relax}=1.81$ s, cartilage within the contact area fully relaxed at the initiation of the unloading portion. Rate-dependent $t_{\rm pull-off}$ indicated that cartilage within the contact area underwent different degrees

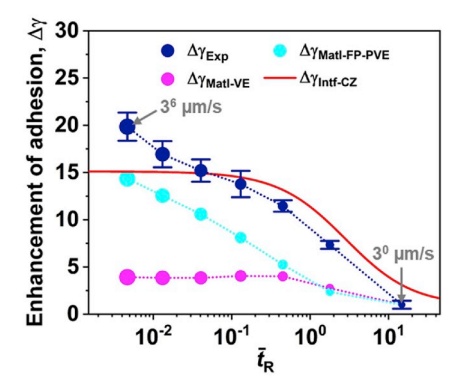


Fig. 5. Comparison of experimental ($\Delta\gamma_{Exp}$) and predicted ($\Delta\gamma_{Matl-VE}$, $\Delta\gamma_{Matl-FP-PVE}$, and $\Delta\gamma_{Intf-CZ}$) enhancements of adhesion. The size of a symbol reflects the magnitude of loading rate (e.g., the smallest size: 3^0 μm/s and the largest size: 3^6 μm/s). The error bars show the standard deviations.

of recovery during unloading. In particular, $t_{pull-off} = 26.67 \pm 9.69 \, \text{s}$ at $3^0 \, \mu \text{m/s}$ was about 15 times longer than τ_{relax} ; this was sufficient time to reach an equilibrium state as observed in $F_{\text{relax}}(t)$ (Fig. 2a). Therefore, cartilage in the vicinity of the indenter had sufficient time to recover during unloading at $3^0 \, \mu \text{m/s}$. In contrast, $t_{\text{pull-off}} = 0.0085 \pm 0.0009$ at $3^6 \, \mu \text{m/s}$ was about 213 times shorter than τ_{relax} and thus cartilage did not have time to recover during unloading. Work of adhesion in cartilage was much smaller at $3^0 \mu m/s$ compared to $3^6 \mu m/s$. As the recovery degree became larger (Fig. 3b), work of adhesion in cartilage became smaller (Fig. 3a). This rate-dependence correlated well with our previous study on cartilage adhesion at different points along the relaxation curve (Han and Eriten, 2018), distinguished from the load profile used in the current study. Work of adhesion at unrelaxed $(0.27\pm0.07 \text{ J/m}^2)$ (fully recovered state)) and relaxed states (5.33±0.96 J/m²) was consistent with that at $3^0 \mu m/s$ (0.36±15 J/m² at $3^0 \mu m/s$) and $3^6 \mu m/s$ $(7.16\pm0.54\,\mathrm{J/m^2})$, respectively. The recovery during unloading is associated with time-dependent phenomena within the bulk material (i. e., PE recovery and VE recovery (Han et al., 2018; Labonte and Federle, 2015; Reale and Dunn, 2017; Tulchinsky and Gat, 2015)) and at the interface (i.e., shape of contact edge (crack) (Barthel and Frétigny, 2009; Greenwood and Johnson, 1981)); it can also be supported by the comparison between the experimental and predicted results (Fig. 5).

The rate dependence of cartilage adhesion ($F_{pull-off}$ and γ_{Exp}) was governed by the apparent load relaxation response (F_{relax}). γ_{Exp} and F_{relax} were compared in the normalized domain (Fig. 4a and b). In this normalized domain, the transition period of cartilage adhesion ($\Delta \gamma_{Exp}$ (\bar{t}_R)) from the relaxed state (i.e., $3^0 \mu m/s$) to the unrelaxed state (i.e., 3⁶ μm/s) corresponded to that of the apparent load relaxation response $(\overline{F}_{\rm relax}(\overline{t}_{\rm R}))$. As a result, a strong correlation between $\Delta \gamma_{\rm Exp}$ and $\overline{F}_{\rm relax}$ was found at the corresponding values of \bar{t}_R (R² = 0.94) (Fig. 4c). The correlation indicated that the apparent load relaxation response $(F_{relax}(t))$ governed the rate dependence of cartilage adhesion ($F_{pull-off}$ and γ_{Exp}). In addition, the correspondence between $\Delta \gamma_{\rm Exp}$ and $\overline{F}_{\rm relax}$ over a wide range of unloading rates reiterated that recovery or relaxation degree of cartilage in the vicinity of the indenter, occurring within the bulk material and at the interface, was associated with the rate dependence of adhesion. Although the correlation cannot provide a direct link between the magnitudes of γ_{Exp} (or $F_{pull-off}$) and F_{relax} , it suggests that rate dependence of cartilage adhesion could be predicted by apparent load relaxation responses.

The relaxation-governed cartilage adhesion provided potential explanations for friction responses of cartilage in the boundary lubrication regime. A previous study showed that GAG-depleted cartilage exhibited stick-slip friction regimes at relatively high sliding speeds (about 4 µm/ s) compared to intact cartilage (about $0.5 \mu m/s$), which was attributed to interpenetration and bridges of molecules (Lee et al., 2013). The current findings (Fig. 4c) combined with our previous study on pre-sliding (static and stick) friction of cartilage (Han and Eriten, 2018) could provide a possible explanation on the shift of stick-slip friction regimes to relatively high sliding speeds in GAG-depleted cartilage. GAG-depleted cartilage exhibits shorter relaxation times than intact cartilage (Nia et al., 2013), and therefore relatively fast sliding rates would be required to separate the adhered contact area before sufficient recovery, leading to relatively high adhesion; higher adhesion can cause higher static (stick) friction in cartilage (Han and Eriten, 2018). In addition, the relaxation-governed cartilage adhesion could explain negative dependence between sliding rates (about 1-1000 µm/s) and kinetic friction in the boundary lubrication regime, reported in a previous study (Coles et al., 2008); the reason for the negative dependence was narrowed down to interfacial effects (e.g., molecular interactions) by eliminating other possible mechanisms of boundary friction (e.g., internal friction, plowing friction, and collisions with asperities) with reasons (Coles et al., 2008). At relatively slow sliding rates, cartilage within the contact area was more likely to have sufficient time to undergo relatively large PVE relaxation (relaxed state), resulting in relatively high adhesion and kinetic friction (Han and Eriten, 2018; Reale and Dunn, 2017). This effect of relaxation-dependent cartilage adhesion on friction responses is not expected at very high sliding rates due to hydrodynamic effects (e.g., sliding-induced recovery of fluid) (Graham et al., 2017).

The rate-dependent enhancement of cartilage adhesion likely originated from the combined effects of the material and interfacial responses. The interpretation of $\Delta \gamma_{Exp}$ based on the predicted trends of $\Delta \gamma_{\text{Matl-VE}}$, $\Delta \gamma_{\text{Matl-FP-PVE}}$, and $\Delta \gamma_{\text{Intf-CZ}}$ provided additional insight into possible origins underlying the rate-dependent enhancement of cartilage adhesion (Fig. 5). $\Delta \gamma_{Exp}$ had a maximum value of about 20 and increased in a linear fashion on a logarithmic time scale (Fig. 5). The complete inconsistency between $\Delta\gamma_{Exp}$ and $\Delta\gamma_{Matl\text{-VE}}$ suggested that the enhancement of cartilage adhesion cannot only be explained with a VE material response. The better agreement between $\Delta \gamma_{Exp}$ and $\Delta \gamma_{Intf-CZ}$ suggested that VE relaxation during interfacial peeling accounts for significant portion of the enhancement of $\Delta \gamma_{Exp}$. This result was consistent with the elastomeric adhesive contact; adhesion in the elastomeric contact strongly depended on loading rates, and this enhancement was explained by imposing the VE dissipation at the edge of the contact area via the introduction of a cohesive zone (Barthel and Frétigny, 2009). The consistency between $\Delta \gamma_{Exp}$ and $\Delta \gamma_{Intf-CZ}$ in the normalized time domain also implied that t_r was similar to $t_{pull-off}$, indicating that the crack propagation velocity at the edge of the contact area was associated with the unloading rate of the indenter. This assumption is in line with observations of a previous study on rate dependence of wet biological adhesives in insects (Labonte and Federle, 2015); where the experimentally observed crack propagation velocity at the edge of the contact region increased with an increasing unloading rate, exhibiting an approximately linear correlation. Even though $\Delta \gamma_{\text{Intf-CZ}}$ provided a better prediction of $\Delta \gamma_{Exp}$ compared to $\Delta \gamma_{Matl-VE}$, $\Delta \gamma_{Intf-CZ}$ reached a plateau at around $3^4\,\mu\text{m/s}$ and failed to explain the increasing trend of $\Delta\gamma_{Exp}$ in the relatively fast unloading rates (i.e., $3^5 \,\mu\text{m/s}$ - $3^6 \,\mu\text{m/s}$). In contrast to $\Delta\gamma_{Intf\text{-}CZ}$ and $\Delta\gamma_{Matl\text{-}VE},\,\Delta\gamma_{Matl\text{-}FP\text{-}PVE}$ showed an increasing trend over a wide range of unloading rates. This trend of $\Delta \gamma_{Matl-FP-PVE}$ was consistent with $\Delta \gamma_{\rm Exp}$, suggesting that negative fluid pressure build-up within the contact area during unloading contributes more to rate-dependent adhesion at fast unloading rates (Tulchinsky and Gat, 2015). Considering ultrastructural similarities between hydrogels and cartilage, a recent study on the effect of fluid pressure on hydrogel adhesion (Reale and Dunn, 2017) supported the results of $\Delta \gamma_{Matl-FP-PVE}$. In addition, when the contact perimeter is considered as a crack (Labonte and Federle, 2015; Shull, 2002), the rate-dependent contribution of the bulk dissipation on cartilage adhesion can be characterized with an empirical power-law relation (Labonte and Federle, 2015; Shull, 2002). The empirical power-law relation for cartilage adhesion suggested that cartilage and hydrogel (Sun et al., 2017) exhibit similar trends in the effect of the bulk dissipation on the energy release rate (Supplementary Fig. 3), supporting the contribution of fluid pressure on cartilage adhesion as observed in hydrogels (Reale and Dunn, 2017). However, the differences in the values of $\Delta \gamma_{\text{Matl-FP-PVE}}$ and $\Delta \gamma_{\text{Exp}}$ implied that a material response was not sufficient to explain $\Delta \gamma_{Exp}$ and interfacial peeling was essential. In conclusion, the models with the bulk-only or interface-only mechanisms could not simulate the adhesion enhancement observed experimentally, $\Delta \gamma_{Exp}$. However, it was suggested that the combination of negative fluid pressure and VE peeling at the interface might be necessary to explain the rate-dependent enhancement of cartilage adhesion ($\Delta \gamma_{Exp}$) over a wide range of unloading rates.

Although these findings filled gaps in knowledge on rate-dependent cartilage adhesion, this study has some limitations. The experimental configurations do not represent *in vivo* conditions. In particular, a rigid spherical indenter was used as a counterpart instead of cartilage. However, this setup allowed investigating the effect of unloading rates on cartilage adhesion under the well-defined contact area. The use of a spherical indenter creates non-uniform deformation. The use of a flatended indenter would allow more uniform deformations. Mechanisms

of rate-dependent cartilage adhesion can be further understood by obtaining in-situ images of contact interfaces at different unloading rates (Creton and Ciccotti, 2016; Labonte and Federle, 2015). For effective image acquisition, a flat-faced indenter would be a good choice as unloading is applied to uniformly deformed cartilage. The tests were only conducted in DBPS solution and therefore do not represent the effect of synovial fluid on cartilage adhesion. The depth-dependent properties of cartilage were not considered in the FE models to minimize the number of fitting parameters; the sacrifice of the depth-dependent properties was reasonable as the solid matrix of immature cartilage (5–6 month old) is relatively homogeneous (Gannon et al., 2015). Notwithstanding, the predictions by the models aided in examining possible mechanisms governing the experimentally observed enhancement of cartilage adhesion.

5. Conclusions

This study investigated rate-dependent cartilage adhesion from preto post-relaxation timescales of cartilage. The adhesion tests with a spherical indenter effectively provided the rate dependence of cartilage adhesion over a wide range of unloading rates and the corresponding load relaxation responses. The wide range of unloading rates revealed the transitional responses of cartilage adhesion from relaxed to unrelaxed states, accompanied by a large adhesion enhancement of about 20 times. These responses correlated with the load relaxation responses. The correlation suggested that the rate dependence of cartilage adhesion can be predicted by the degree of relaxation in the tissue. These results also indicated that cartilage within the contact area had sufficient time to recover (or relax) at the slow unloading rates, resulting in relatively lower adhesion. The comparison between the experimental and predicted results suggested that combined effects of VE peeling of interface and negative fluid pressure (poroelasticity) within the contact area were required to explain the experimentally observed enhancement of cartilage adhesion. These findings fill the gap in the experimental observation of rate-dependent cartilage adhesion from relaxed to unrelaxed states and extend understanding of rate-dependent adhesion mechanisms in cartilage. They also provide additional insights into friction responses and stick-induced damage in cartilage especially in adhesiondominated contact regimes (e.g., boundary lubrication).

Acknowledgment

Funding from the National Science Foundation (CMMI-DCSD-1662456) is gratefully acknowledged. The authors are grateful to Shannon K. Walsh for helpful discussions on statistical analysis.

Appendix A. Supplementary data

Supplementary data to this article can be found online at https://doi.org/10.1016/j.jmbbm.2019.103493.

References

Ahn, D., Shull, K.R., 1996. JKR studies of acrylic elastomer adhesion to glassy polymer substrates. Macromolecules 29, 4381–4390. https://doi.org/10.1021/ma9518924.

Andriotis, O.G., Desissaire, S., Thurner, P.J., 2018. Collagen fibrils: nature's highly tunable nonlinear springs. ACS Nano 12, 3671–3680. https://doi.org/10.1021/acsnano.8b00837.

Ateshian, G.A., Warden, W.H., Kim, J.J., Grelsamer, R.P., Mow, V.C., 1997. Finite deformation biphasic material properties of bovine articular cartilage from confined compression experiments. J. Biomech. 30, 1157–1164. https://doi.org/10.1016/ S0021-9290(97)85606-0.

Barthel, E., Frétigny, C., 2009. Adhesive contact of elastomers: effective adhesion energy and creep function. J. Phys. Appl. Phys. 42, 195302. https://doi.org/10.1088/0022-3727/42/10/195302

Bonnevie, E.D., Delco, M.L., Bartell, L.R., Jasty, N., Cohen, I., Fortier, L.A., Bonassar, L.J., 2018. Microscale frictional strains determine chondrocyte fate in loaded cartilage. J. Biomech. 74, 72–78. https://doi.org/10.1016/j.jbiomech.2018.04.020.

- Cai, L.-H., Kodger, T.E., Guerra, R.E., Pegoraro, A.F., Rubinstein, M., Weitz, D.A., 2015. Soft poly(dimethylsiloxane) elastomers from architecture-driven entanglement free design. Adv. Mater. 27, 5132–5140. https://doi.org/10.1002/adma.201502771.
- Chan, S.M.T., Neu, C.P., Komvopoulos, K., Reddi, A.H., 2011. Dependence of nanoscale friction and adhesion properties of articular cartilage on contact load. J. Biomech. 44, 1340–1345. https://doi.org/10.1016/j.jbiomech.2011.01.003.
- Chiravarambath, S., Simha, N.K., Namani, R., Lewis, J.L., 2008. Poroviscoelastic cartilage properties in the mouse from indentation. J. Biomech. Eng. 131 https://doi. org/10.1115/1.3005199, 011004-011004-9.
- Coles, J.M., Blum, J.J., Jay, G.D., Darling, E.M., Guilak, F., Zauscher, S., 2008. In situ friction measurement on murine cartilage by atomic force microscopy. J. Biomech. 41, 541–548. https://doi.org/10.1016/j.jbiomech.2007.10.013.
- Creton, C., Ciccotti, M., 2016. Fracture and adhesion of soft materials: a review. Rep. Prog. Phys. 79, 046601 https://doi.org/10.1088/0034-4885/79/4/046601.
- Deruelle, M., Leger, L., Tirrell, M., 1995. Adhesion at the solid-elastomer interface: influence of the interfacial chains. Macromolecules 28, 7419–7428. https://doi.org/
- DiSilvestro, M.R., Zhu, Q., Wong, M., Jurvelin, J.S., Suh, J.-K.F., 2000. Biphasic poroviscoelastic simulation of the unconfined compression of articular cartilage: I—simultaneous prediction of reaction force and lateral displacement. J. Biomech. Eng. 123, 191–197. https://doi.org/10.1115/1.1351890.
- Gannon, A.R., Nagel, T., Bell, A.P., Avery, N.C., Kelly, D.J., 2015. Postnatal changes to the mechanical properties of articular cartilage are driven by the evolution of its collagen network. Eur. Cells Mater. 29, 105–121 discussion 121-123.
- Geuzaine, C., Remacle, J.-F., 2009. Gmsh: a 3-D finite element mesh generator with builtin pre- and post-processing facilities. Int. J. Numer. Methods Eng. 79, 1309–1331. https://doi.org/10.1002/nme.2579.
- Graham, B.T., Moore, A.C., Burris, D.L., Price, C., 2017. Sliding enhances fluid and solute transport into buried articular cartilage contacts. Osteoarthr. Cartil. 25, 2100–2107. https://doi.org/10.1016/j.joca.2017.08.014.
- Greenwood, J.A., Johnson, K.L., 1981. The mechanics of adhesion of viscoelastic solids. Philos. Mag. A 43, 697–711. https://doi.org/10.1080/01418618108240402.
- Han, E., Chen, S.S., Klisch, S.M., Sah, R.L., 2011. Contribution of proteoglycan osmotic swelling pressure to the compressive properties of articular cartilage. Biophys. J. 101, 916–924. https://doi.org/10.1016/j.bpj.2011.07.006.
- Han, G., Eriten, M., 2018. Effect of relaxation-dependent adhesion on pre-sliding response of cartilage. R. Soc. Open Sci. 5, 172051. https://doi.org/10.1098/ rsos.172051.
- Han, G., Eriten, M., Henak, C.R., 2019. Rate-dependent crack nucleation in cartilage under microindentation. J. Mech. Behav. Biomed. Mater. 96, 186–192. https://doi. org/10.1016/j.jmbbm.2019.04.015.
- Han, G., Hess, C., Eriten, M., Henak, C.R., 2018. Uncoupled poroelastic and intrinsic viscoelastic dissipation in cartilage. J. Mech. Behav. Biomed. Mater. 84, 28–34. https://doi.org/10.1016/j.jmbbm.2018.04.024.
- Huang, C.Y., Mow, V.C., Ateshian, G.A., 2001. The role of flow-independent viscoelasticity in the biphasic tensile and compressive responses of articular cartilage. J. Biomech. Eng. 123, 410–417.
- Huang, C.-Y., Soltz, M.A., Kopacz, M., Mow, V.C., Ateshian, G.A., 2003. Experimental verification of the roles of intrinsic matrix viscoelasticity and tension-compression nonlinearity in the biphasic response of cartilage. J. Biomech. Eng. 125, 84–93. https://doi.org/10.1115/1.1531656.
- Johnson, K.L., Kendall, K., Roberts, A.D., 1971. Surface energy and the contact of elastic solids. Proc. R. Soc. Lond. Math. Phys. Eng. Sci. 324, 301–313. https://doi.org/ 10.1098/rspa.1971.0141.
- Kempson, G.E., Freeman, M.a.R., Swanson, S.a.V., 1968. Tensile properties of articular cartilage. Nature 220, 1127–1128. https://doi.org/10.1038/2201127b0.
- Labonte, D., Federle, W., 2015. Rate-dependence of wet' biological adhesives and the function of the pad secretion in insects. Soft Matter 11, 8661–8673. https://doi.org/ 10.1039/C5SM01496D.
- Lai, Y., Hu, Y., 2017. Unified solution for poroelastic oscillation indentation on gels for spherical, conical and cylindrical indenters. Soft Matter 13, 852–861. https://doi. org/10.1039/C6SM02341J.

- Lakes, P.R., 2009. Viscoelastic Materials, 1 edition. Cambridge University Press, Cambridge: New York.
- Lee, D.W., Banquy, X., Israelachvili, J.N., 2013. Stick-slip friction and wear of articular joints. Proc. Natl. Acad. Sci. 110, E567–E574. https://doi.org/10.1073/ pnas.1222470110.
- Li, L.P., Korhonen, R.K., Iivarinen, J., Jurvelin, J.S., Herzog, W., 2008. Fluid pressure driven fibril reinforcement in creep and relaxation tests of articular cartilage. Med. Eng. Phys. 30, 182–189. https://doi.org/10.1016/j.medengphy.2007.03.001.
- Maas, S.A., Ellis, B.J., Ateshian, G.A., Weiss, J.A., 2012. FEBio: finite elements for biomechanics. J. Biomech. Eng. 134, 011005 https://doi.org/10.1115/1.4005694.
- Mak, A.F., 1986. The apparent viscoelastic behavior of articular cartilage—the contributions from the intrinsic matrix viscoelasticity and interstitial fluid flows. J. Biomech. Eng. 108, 123–130. https://doi.org/10.1115/1.3138591.
- Maroudas, A., Wachtel, E., Grushko, G., Katz, E.P., Weinberg, P., 1991. The effect of osmotic and mechanical pressures on water partitioning in articular cartilage. Biochim. Biophys. Acta BBA - Gen. Subj. 1073, 285–294. https://doi.org/10.1016/ 0304-4165(91)90133-2.
- Mow, V.C., Ratcliffe, A., Robin Poole, A., 1992. Cartilage and diarthrodial joints as paradigms for hierarchical materials and structures. Biomaterials 13, 67–97. https://doi.org/10.1016/0142-9612(92)90001-5.
- Nia, H., Bozchalooi, I.S., Li, Y., Han, L., Hung, H.-H., Frank, E., Youcef-Toumi, K., Ortiz, C., Grodzinsky, A., 2013. High-bandwidth AFM-based rheology reveals that cartilage is most sensitive to high loading rates at early stages of impairment. Biophys. J. 104, 1529–1537. https://doi.org/10.1016/j.bpj.2013.02.048.
- Nia, H., Han, L., Li, Y., Ortiz, C., Grodzinsky, A., 2011. Poroelasticity of cartilage at the nanoscale. Biophys. J. 101, 2304–2313. https://doi.org/10.1016/j.bpj.2011.09.011.
- Nia, H., Han, L., Soltani Bozchalooi, I., Roughley, P., Youcef-Toumi, K., Grodzinsky, A.J., Ortiz, C., 2015. Aggrecan nanoscale solid–fluid interactions are a primary determinant of cartilage dynamic mechanical properties. ACS Nano 9, 2614–2625. https://doi.org/10.1021/nn5062707.
- Reale, E.R., Dunn, A.C., 2017. Poroelasticity-driven lubrication in hydrogel interfaces. Soft Matter 13, 428–435. https://doi.org/10.1039/C6SM02111E.
- Shull, K.R., 2002. Contact mechanics and the adhesion of soft solids. Mater. Sci. Eng. R Rep. 36, 1–45. https://doi.org/10.1016/S0927-796X(01)00039-0.
- Soulhat, J., Buschmann, M.D., Shirazi-Adl, A., 1999. A fibril-network-reinforced biphasic model of cartilage in unconfined compression. J. Biomech. Eng. 121, 340–347. https://doi.org/10.1115/1.2798330.
- Suh, J.-K., 1996. Dynamic unconfined compression of articular cartilage under a cyclic compressive load. Biorheology 33, 289–304. https://doi.org/10.3233/BIR-1996-334-501.
- Sun, T.L., Luo, F., Hong, W., Cui, K., Huang, Y., Zhang, H.J., King, D.R., Kurokawa, T., Nakajima, T., Gong, J.P., 2017. Bulk Energy Dissipation Mechanism for the Fracture of Tough and Self-Healing Hydrogels, vol. 50, pp. 2923–2931.
- Torzilli, P.A., 1985. Influence of cartilage conformation on its equilibrium water partition. J. Orthop. Res. 3, 473–483. https://doi.org/10.1002/jor.1100030410.
- Tulchinsky, A., Gat, A.D., 2015. Viscous–poroelastic interaction as mechanism to create adhesion in frogs' toe pads. J. Fluid Mech. 775, 288–303. https://doi.org/10.1017/ ifm 2015 293
- Wilson, W., van Donkelaar, C.C., van Rietbergen, B., Huiskes, R., 2005. A fibrilreinforced poroviscoelastic swelling model for articular cartilage. J. Biomech. 38, 1195–1204. https://doi.org/10.1016/j.jbiomech.2004.07.003.
- Wong, B.L., Bae, W.C., Chun, J., Gratz, K.R., Lotz, M., Sah, R.L., 2008. Biomechanics of cartilage articulation: effects of lubrication and degeneration on shear deformation. Arthritis Rheum. 58, 2065–2074. https://doi.org/10.1002/art.23548.
- Yamaguchi, T., Creton, C., Doi, M., 2018. Simple model on debonding of soft adhesives. Soft Matter 14, 6206–6213. https://doi.org/10.1039/C8SM00723C.
- Yang, L., van der Werf, K.O., Dijkstra, P.J., Feijen, J., Bennink, M.L., 2012.
 Micromechanical analysis of native and cross-linked collagen type I fibrils supports the existence of microfibrils. J. Mech. Behav. Biomed. Mater. 6, 148–158. https://doi.org/10.1016/j.jmbbm.2011.11.008.